Highly Controllable and Efficient Synthesis of Mixed-Halide CsPbX₃ (X = Cl, Br, I) Perovskite QDs toward the Tunability of Entire Visible Light

Ying Su,[†,‡,§] Xuejiao Chen,[†,‡,§] Wenyu Ji,[†] Qinghui Zeng,*,[†] Zhongyuan Ren,[†] Zisheng Su,[†] and Lei Liu[†]

[†]State Key Laboratory of Luminescence and Applications, Changchun Institute of Optics, Fine Mechanics and Physics, Chinese Academy of Sciences, Dong_Nanhu Road 3888, Changchun 130033, P. R. China

[‡]University of Chinese Academy of Sciences, Beijing 100049, P. R. China

Ⓢ *Supporting Information*

ABSTRACT: CsPbX₃ (X = Cl, Br, I) perovskite quantum dots (PQDs) have been intensively investigated on photoelectric devices due to their superior optical properties. To date, the stability of CsPbX₃ PQDs is still an open challenge. The previous mixed-halide CsPbX₃ PQDs were generally obtained via the anion-exchange method at 40 °C. Here, the single- and mixed-halide CsPbX₃ PQDs are synthesized at high temperature via the hot injection technique. The surface ligands could thus be strongly coordinated onto the surface of the PQDs, which dramatically improve the optical properties of the PQDs. The resulting CsPbX₃ PQDs have high quantum yield (QY, 40−95%), narrow full width at half-maximum (FWHM) (the narrowest FWHM <10 nm), tunable band gap (408−694 nm), and highly strong photostability. The variation of their emission peaks upon anion atoms is well-supported by the theoretical band gaps calculated by the density functional theory calculations with the alloy formula correction. Hence, these PQDs show great potential as good candidates for photoelectric devices.

KEYWORDS: all-inorganic CsPbX₃ (X = Cl, Br, I) perovskite QDs, hot injection technique, mixed-halide CsPbX₃ perovskite QDs, narrow FWHM, photostability
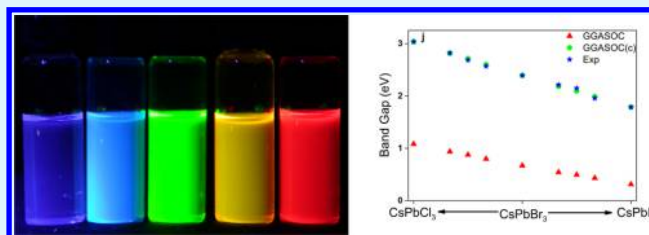
1. INTRODUCTION

Colloidal semiconductor quantum dots (QDs), due to their unique optical properties, have been widely applied in the biomedical field, optoelectronics research field, and so on.[1−4] Recently, due to the facile synthesis method and narrow emission spectrum properties, the CsPbX₃ (X = Cl, Br, I) perovskite QDs (PQDs) have gradually attracted much attention, especially on their applications to the photoelectrical devices, e.g., light emitting diodes (LEDs) lighting, displays, lasers, and solar cells.[5−8] As compared with the hybrid organic−inorganic PQDs, the all-inorganic CsPbX₃ PQDs not only possess excellent quality similar to the traditional all-inorganic II−VI and III−V race QDs but also present the resistance to oxidation, moisture resistance property, high stability, etc. Thus, they certainly merit a full prospect of their future applications in the optoelectronic field. Therefore, the whole-visible-light CsPbX₃ PQDs further attracted the attention of the researchers. Until now, the stability of the whole-visible-light CsPbX₃ PQDs is still an open problem. On the basis of the successful experience of the traditional II−VI CdSe QDs, the surface ligand (including the capability of coordination, the amount of the coordinated ligand, etc.) is a crucial factor to influence the stability of the QDs. In fact, the effects of surface ligands are mainly reflected from three aspects:[9,10] first, the large surface-to-volume ratio of QDs results in ample fluorescent quenching centers at the nanocrystal surface and the surface ligand could passivate the dangling bonds and prevent nonradiative recombination at surface trap states;[11] second, the surface ligand could prevent the QDs from aggregation;[12,13] finally, the growth kinetics of the QDs is, to a large extent, a function of the affinity of the precursors for the capping molecules and the stability of the capping ligand precursor intermediate complex.[14]

At present, the whole-visible-light CsPbX₃ PQDs were obtained generally by preparing the mixed-halide CsPbIₓBr₃₋ₓ or CsPbBrₓCl₃₋ₓ PQDs after an anion exchange of single-halide CsPbX₃ with methylmagnesium halide at 40 °C.[15] However, it is reported subsequently that the phase separation (including the distortion of the cubic phase and expansion or shrinkage of the lattice constant) would lead to the change of the optical and electrical properties, especially leading to poor stability and half of loss for the quantum yields (QYs),[16] which will inevitably restrict their applications in both biomedical and optoelectronic fields. Meanwhile, because of the fast anion-exchange process

and unexpectable control synthesis, the resulting mixed-halide $CsPbI_xBr_{3-x}$ or $CsPbBr_xCl_{3-x}$ PQDs often show an unsatisfactory optical property, such as weak excitonic absorption peak, inferior Gaussian distribution photoluminescence (PL) spectra, wide full width at half-maximum (FWHM), etc. In addition, the highly toxic *n*-trioctylphosphine (TOP) ligand was unavoidably used in the synthesis of chloride-doped $CsPbCl_3$ PQDs,[15] which will greatly restrict the future application of the PQDs on the extensive green production. Because the investigation of PQDs is just at the start-up stage, only a few studies[17−19] on the theoretical calculation using different methods, including supercell, the alloy-theoretic automated toolkit (ATAT) code, and virtual crystal approximation, have been carried out to investigate the properties of hybrid organic−inorganic PQDs. Therefore, there is an impending demand on the relative theoretical calculation including spin−orbital coupling (SOC) research to directly verify and compare with the experimental results of all-inorganic halide perovskite QDs.

In this work, the single- and mixed-halide $CsPbX_3$ PQDs were directly synthesized at high temperature via the hot injection technique after an accurate designation and calculation of the raw material and precursor solution's concentration. Because the surface ligands were coordinated at high temperature rather than via the published method using the anion-exchange technique at 40 °C. The surface ligands could be strongly coordinated onto the surface of the PQDs, which will certainly improve the optical properties and enhance the stability of the resulting $CsPbI_xBr_{3-x}$ or $CsPbBr_xCl_{3-x}$ PQDs. The friendly double ligands of oleic acid (OA)/oleylamine (OAm) were used instead of the traditional OA/OAm/TOP mixture to synthesize the PQDs. As compared with the previous strict synthesis processes that needed vacuumization or/and glovebox equipment, a facile method that only need argon as the protective gas was provided to prepare high-quality PQDs through accurately controlling the ratio of different halide atoms and the hot injection technique. The resulting PQDs have high QY (the highest QY up to 95%), narrow FWHM (the narrowest FWHM <10 nm), tunable band gap (408−694 nm) in the whole-visible-light window, and rather strong photostability, which will bring them wide applications in the photoelectric devices such as LEDs and solar cells. Moreover, we have constructed the crystal models of mixed-halide PQDs with the $1 \times 1 \times 2$ supercell, calculated the band structures, and compared the band gaps with peaks in PL spectra. The theoretical direct band gaps are in good agreement with the experimental results.

2. EXPERIMENTAL SECTION

2.1. Chemicals and Reagents. Cesium carbonate (Cs_2CO_3, 99.9%), oleic acid (OA, ≥99%), 1-octadecene (ODE, 90%), oleylamine (OAm, ≥98%), lead chloride ($PbCl_2$, 99.999%), lead bromide ($PbBr_2$, 99.999%), and lead iodide (PbI_2, 99.999%) were purchased from Sigma-Aldrich. Toluene (≥95%) and hexane (≥95%) were purchased from Beijing Chemical Works. All of the reagents were used without further purification.

2.2. Preparation of Cesium Oleate Precursors. First, Cs_2CO_3 (0.391 g, 1.2 mmol), OA (1.27 mL, 4 mmol), and ODE (18.73 mL) were added into a 50 mL 3-neck flask. Here, the oleic acid was in excess of the Cs element to make a sufficient reaction of Cs_2CO_3 salt. After a 60 min stirring under argon flowing at 120 °C, this mixture was heated to 160 °C to make a clear solution. After about 30 min reaction, Cs_2CO_3 was reacted with OA and the cesium oleate precursors could be prepared. Because cesium oleate precipitates out

of ODE at room temperature, it must be preheated to above 80 °C before injection.

2.3. Synthesis of $CsPbX_3$ (X = Cl, Br, or I) QDs. Typically, in a 100 mL three-neck flask, 0.4 mmol PbX_2 (0.1112 g for $PbCl_2$, 0.149 g for $PbBr_2$, or 0.1844 g for PbI_2) was added, followed by the addition of 24 mL of ODE. After a 30 min stirring under argon flowing at room temperature, this mixture was heated to 120 °C for another 30 min. Then OA (1 mL) and OAm (3 mL) were injected into the reaction bottle by a syringe needle. After a few seconds' stirring, PbX_2 could be completely solubilized and a clear solution was obtained. Then, the temperature was raised to 180 °C and the cesium oleate precursor (2 mL) was quickly injected. After a designed reaction time, the growth of the NPs was terminated and the reaction mixture was cooled down by an ice−water bath for the next purification process. Simply, the obtained NPs were centrifuged by adding about 30 mL of toluene at 9000 rpm (a centrifugal force of 9000*g*) for 10 min. After centrifugation, the supernatant was poured off and the NPs at the bottom of the centrifuge tube were redispersed in hexane. This purification process was repeated twice. After the purification, NPs were stored as dispersion in hexane or chloroform. From the field emission scanning electron microscopy (FE-SEM) image, the size of the $CsPbBr_3$ QDs was ca. 12 nm.

2.4. Synthesis of $CsPbBr_xCl_{3-x}$ and $CsPbI_xBr_{3-x}$ QDs. Typically, in a 100 mL three-neck flask, 0.4 mmol PbX_2 (0.0745 g of $PbBr_2$ and 0.0556 g of $PbCl_2$ for $CsPbBr_{1.5}Cl_{1.5}$ perovskite QDs, 0.0922 g of PbI_2 and 0.0745 g of $PbBr_2$ for $CsPbI_{1.5}Br_{1.5}$ perovskite QDs, and 0.0489 g of $PbBr_2$ and 0.0742 g of $PbCl_2$ for $CsPbBr_1Cl_2$ perovskite QDs, etc.) was added, followed by the addition of 24 mL of ODE. After a 30 min stirring under argon flowing at room temperature, this mixture was heated to 120 °C for another 30 min. Then OA (1 mL) and OAm (3 mL) were injected into the reaction bottle by a syringe needle. After a few seconds' stirring, the PbX_2 could be completely solubilized and a clear solution was obtained. Then, the temperature was raised to 180 °C and the cesium oleate precursor (2 mL) was quickly injected. After a designed reaction time, the growth of the NPs was terminated and the reaction mixture was cooled down by an ice−water bath for the next purification process. Simply, the obtained NPs were centrifuged by adding about 30 mL of toluene at 9000 rpm (a centrifugal force of 9000*g*) for 10 min. After centrifugation, the supernatant was poured off and the NPs at the bottom of the centrifuge tube were redispersed in hexane. This purification process was repeated twice. After the purification, NPs were stored as dispersion in hexane or chloroform.

2.5. Computation Method. All crystal structures and electronic properties are calculated on the basis of density functional theory using the Vienna ab initio simulation package (VASP)[20,21] under the generalized gradient approximation (GGA) of Perdew−Burke−Ernzerhof (PBE).[22] The ion cores are described by the projector-augmented wave method.[23,24] The energy cutoff for the plane-wave basis is 500 eV for the entire process, and the residual force is less than 0.001 eV/Å. During the relaxation process, the Brillouin zones are sampled with a $6 \times 6 \times 6$ *k*-point mesh for a unit cell and $6 \times 6 \times 3$ *k*-point mesh for a $1 \times 1 \times 2$ supercell, respectively. We calculate the band structures with/without spin−orbital coupling (SOC).

We construct crystal structures of $CsPb(Br_xCl_{1-x})_3$ and $CsPb(I_xBr_{1-x})_3$ with $x = 0, 1/3, 1/2, 2/3, 1$ using the supercell method with the symmetry condition. The band gaps with SOC are further corrected to match the experimental value according to the alloy formula,[17] which is $\Delta E_g(A_{1-x}B_x) = (1 - x)\Delta E_g(A) + x\Delta E_g(B)$, where $\Delta E_g(A_{1-x}B_x)$ is the alloy $A_{1-x}B_x$ band gap correction and $\Delta E_g(A)$ and $\Delta E_g(B)$ are the band gap corrections for the pure phase of A and B.

2.6. Calculation of QY. PL QY was estimated by comparing the samples with the standard fluorescent dye according to the following formula: $Q_x = Q_r[A_r/A_x][I_r/I_x][n^2_x/n^2_r][D_x/D_r]$, where Q is the QY, A is the absorption intensity at the excitation wavelength, I is the intensity of the excitation light, n is the refractive index, D is the fluorescent integral area, and the subscripts x and r denote the sample and standard.

2.7. Characterization. The morphology, size distribution, and energy-dispersive X-ray results of $CsPbX_3$ PQDs were characterized by field emission scanning electron microscopy (FE-SEM, Hitachi, S-
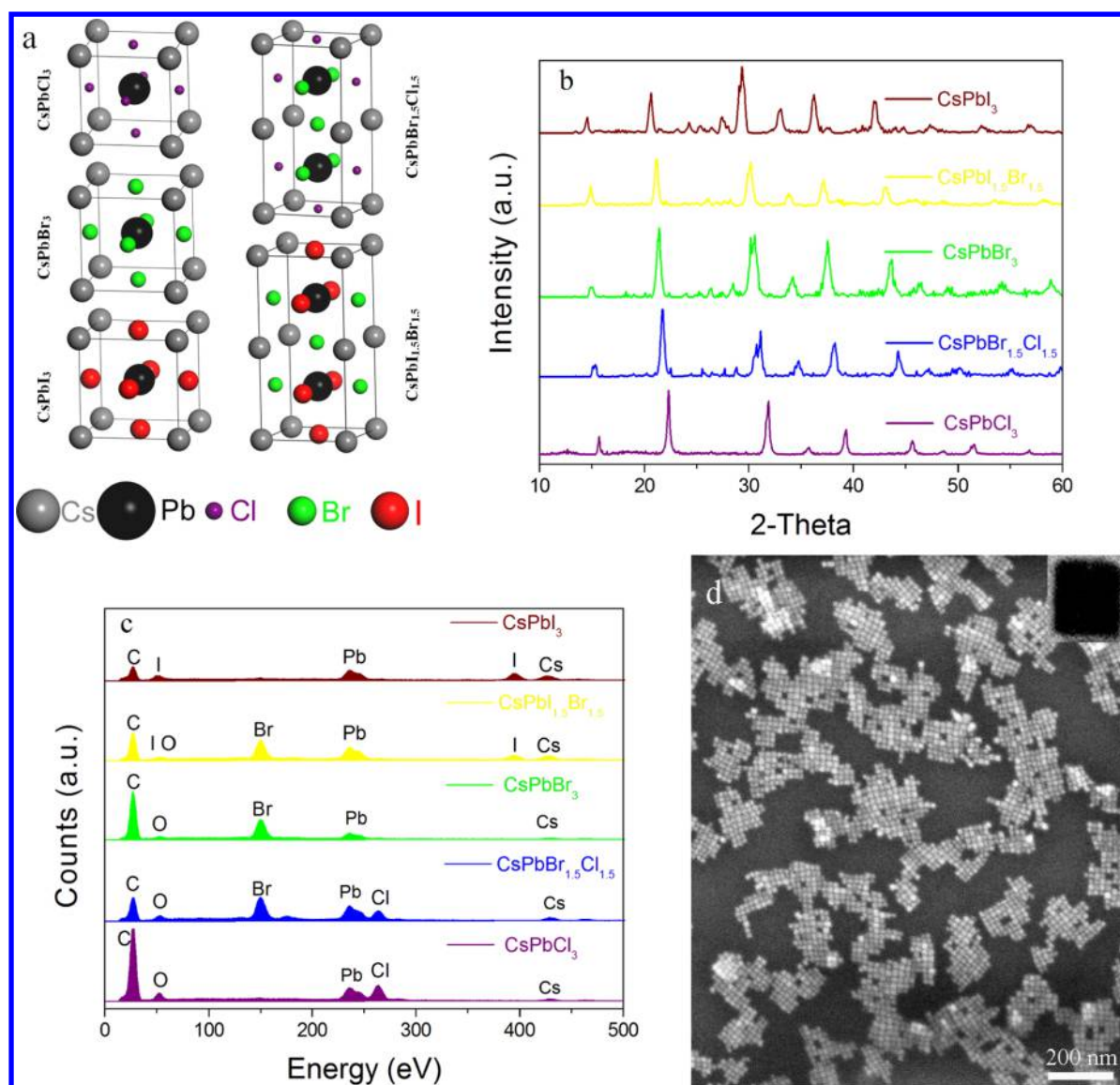
Figure 1. Schematic cubic structures (a), XRD patterns (b), and EDS (c) spectra of the dried $CsPbCl_3$, $CsPbBr_{1.5}Cl_{1.5}$, $CsPbBr_3$, $CsPbI_{1.5}Br_{1.5}$, and $CsPbI_3$ PQDs. FE-SEM image of the $CsPbBr_3$ PQDs (d); the inset is the TEM image of the $CsPbBr_3$ PQDs.

4800), and the voltage is 5 kV. Absorption and PL spectra were measured at indoor temperature by a UV-3101 spectrophotometer and Hitachi F-7000 fluorescence spectrofluorimeter, respectively. X-ray diffraction (XRD) patterns were obtained using a D8 Focus X-ray diffractometer purchased from Bruker Company.

3. RESULTS AND DISCUSSION

3.1. Synthesis and Characterization of Single and Mixed-Halide $CsPbX_3$ PQDs. We have proposed an efficient and facile method to prepare single- and mixed-halide $CsPbX_3$ PQDs. First, the Cs-oleate precursor solution was prepared by adding the Cs_2CO_3 salt and oleic acid in the octadecene solution and reacted at 160 °C. Then, the Cs-oleate precursor solution was injected into a three-neck bottle including the octadecene-solubilized PbX_2 through the hot injection technique and a 3:1 mixture of OAm and OA was selected as the surface ligands to activate the Pb precursor. The schematic reaction equipment is shown in Figure S1 (Supporting Information), and the experimental details can be found in Section 2. Compared with that in the previous classical method reported by Kovalenko et al.,[15,25] the friendly double ligand of

OA/OAm was used instead of the OA/OAm/TOP mixture to synthesize the $CsPbX_3$ PQDs, including the chloride-doped $CsPbCl_3$ PQDs, and no vacuumization or glovebox operation processes are required. The molar ratio of Cs/Pb/X in the previous work[15] was settled as 0.025:0.188:0.376; however, in this work, we have changed the molar ratio to 0.12:0.2:0.4, which may improve the maximum reaction yield from 13 to 60%. It is essential that the Cs/Pb molar ratio is settled as 0.12:0.2 to obtain highly luminescent PQDs. Therefore, the maximum reaction yield is unsuitable to achieve 100% due to the fact that the desired maximum QY can only be obtained when the molar ratio of Cs/Pb is 0.12:0.2, rather than 0.2:0.2.

$CsPbX_3$ crystallizes in a cubic, tetragonal, and orthorhombic phase from high to low temperature with the symmetry of crystal structure down. Recently, the quantum dot, film, and nanoplate of $CsPbX_3$ own the cubic phase at room temperature, which can be attributed to the nanocrystal surface, high synthesis temperature, and surface energy.[25−27] Here, the $CsPbX_3$ PQDs prepared by our method still maintain the cubic phase, in which $CsPbX_3$ is composed of five atoms with halide
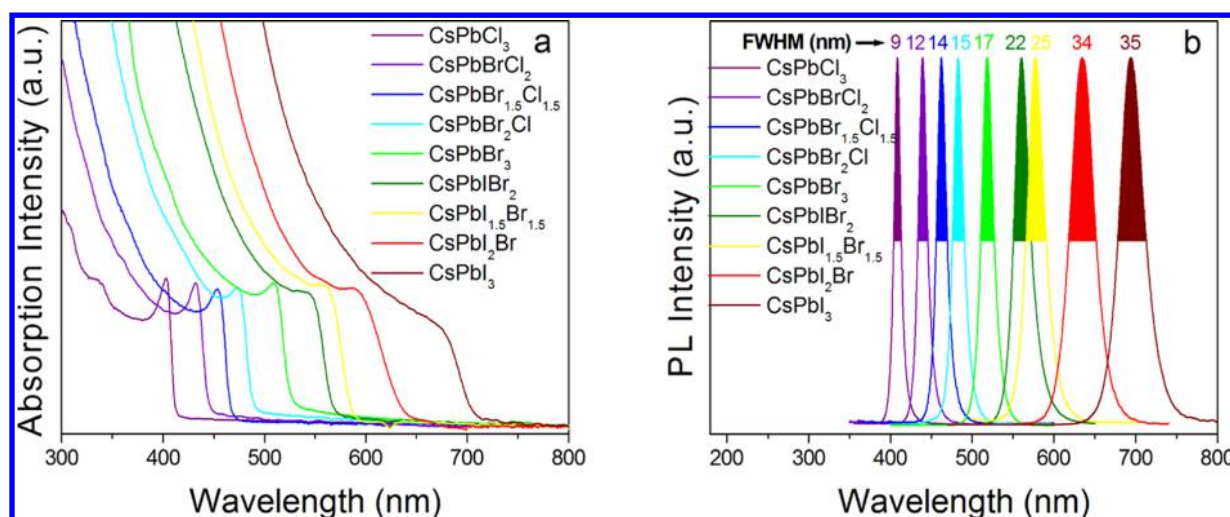
Figure 2. Normalized absorption (a) and emission (b) spectra of CsPbCl$_3$, CsPbBrCl$_2$, CsPbBr$_{1.5}$Cl$_{1.5}$, CsPbBr$_2$Cl, CsPbBr$_3$, CsPbIBr$_2$, CsPbI$_{1.5}$Br$_{1.5}$, CsPbI$_2$Br, and CsPbI$_3$ PQD solutions synthesized in this work.
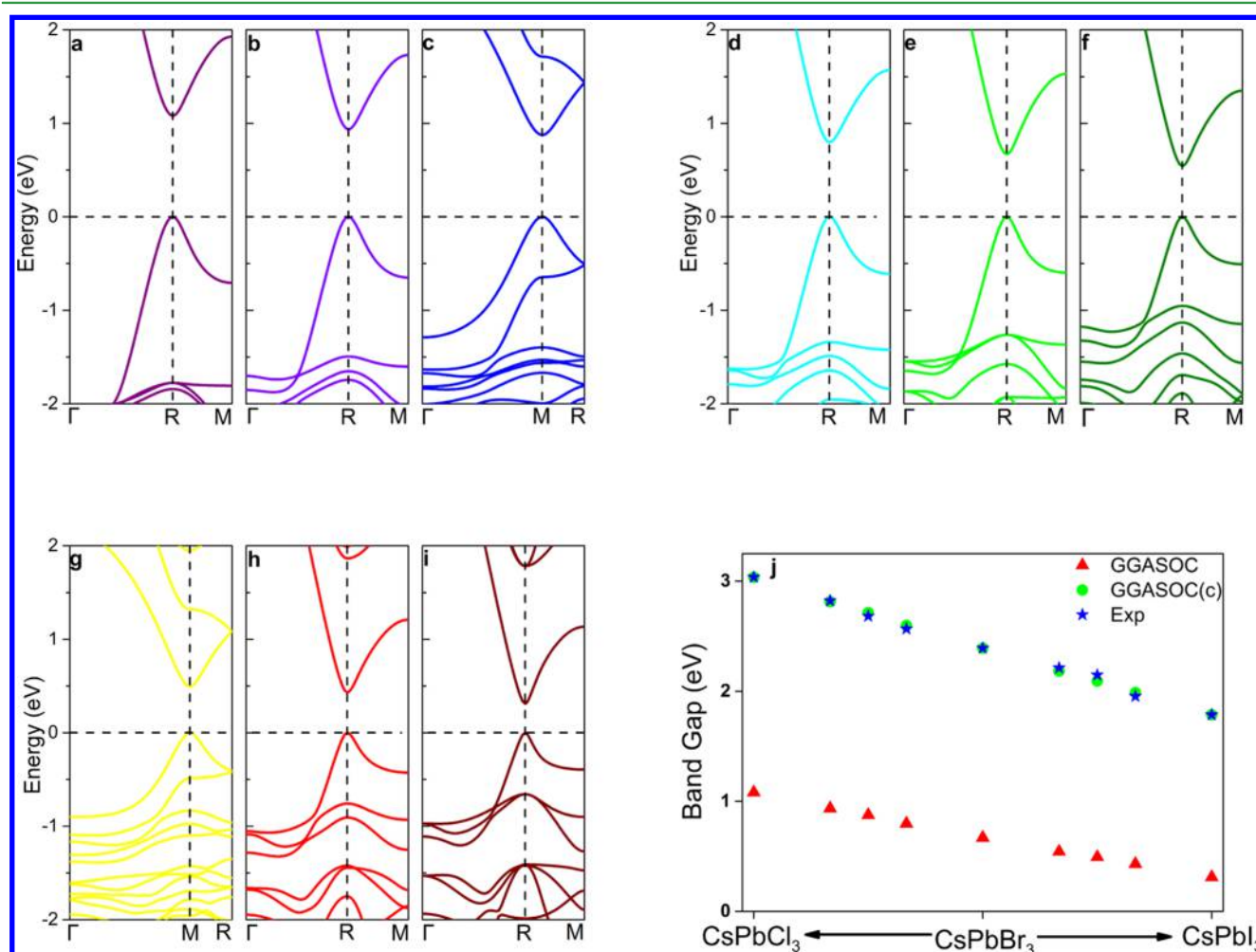
Figure 3. Band structure of (a) CsPbCl$_3$, (b) CsPbBrCl$_2$, (c) CsPbBr$_{1.5}$Cl$_{1.5}$, (d) CsPbBr$_2$Cl, (e) CsPbBr$_3$, (f) CsPbIBr$_2$, (g) CsPbI$_{1.5}$Br$_{1.5}$, (h) CsPbI$_2$Br, and (i) CsPbI$_3$ with spin−orbital coupling. The valence band maximum is set as zero. The band gap of different mixed-ratio CsPbX$_3$ PQDs (j). The red triangle represents the values of GGA with SOC. The green circle represents the values of GGA with SOC corrected by the alloy correction formula. The blue star represents the experimental values.

lead octahedral and Cs$^+$ sharing the corner of the regular octahedral. Figure 1a shows the crystal structures of the CsPbCl$_3$, CsPbBr$_3$, and CsPbI$_3$ PQDs and CsPbBr$_{1.5}$Cl$_{1.5}$ and CsPbI$_{1.5}$Br$_{1.5}$ constructed using the 1 × 1 × 2 supercell method. The relative X-ray diffraction (XRD) spectra of the PQDs are shown in Figure 1b; as expected, the CsPbX$_3$ PQDs present

obviously the cubic phase and the hybrid halide inorganic PQDs show similarly a cubic phase with a little shift of the position and broadening for the 2θ angles, owing to the differences in the ionic radius of halide atoms. As the halide ion was changed from Cl^- to Br^- and to I^-, the 2θ angle gradually shifts to a small angle direction regularly, which phenomenon is in accordance with the previous studies.[15,25] When the dopant halogen ions are changed from I^- to Br^- or Cl^-, the size of the crystal cell is reduced, leading to a shift of the diffraction peaks toward larger angles and vice versa. The shift extent will also be influenced by the relative content of the dopant halogen ions. All of the XRD spectra of $CsPbX_3$ PQDs show the broadening peak due to the small size (~10 nm) of $CsPbX_3$ perovskite QDs. Element analysis was performed using an energy-dispersive X-ray spectrometer (EDS) to confirm the elemental composition ratios of the $CsPbCl_3$, $CsPbBr_{1.5}Cl_{1.5}$, $CsPbBr_3$, $CsPbI_{1.5}Br_{1.5}$, and $CsPbI_3$ PQDs (Figure 1c). The detailed element ratio of Cs, Pb, and halogen ions is shown in Table S1. After the calculation and analysis, the experimental ratios are in good agreement with the expected ones. These results demonstrated the highly controllable and efficient synthesis of the PQDs via the hot injection technique. As shown in Figure 1d, both the field emission scanning electron microscope (FE-SEM) and transmission electron microscope (TEM) images present the cubic shape of $CsPbBr_3$ PQDs in morphology and the homogeneous synthesis method. After statistical analysis, the size of the prepared $CsPbBr_3$ PQDs is mainly about 12 nm.

The absorption and emission spectra of the $CsPbX_3$ PQD solution prepared with our hot injection technique exhibit the high absorption coefficient, narrow FWHM, tunable band gaps, and high QY. As described in Figure 2, both the single- and mixed-halide $CsPbX_3$ QDs show the absorption spectra with a clear excitonic absorption peak, which proves efficiently the homogeneity of the prepared PQDs. The narrow FWHM of 9−35 nm further evidenced this result (see Figure S2a). Importantly, the FWHM of the PL spectrum for the $CsPbCl_3$ PQDs obtained by our method is only 9 nm, which is <10 nm, and is the smallest FWHM value ever published for the QD dispersion solution sample until now. In addition, the FWHM of the other single- and mixed-halide $CsPbX_3$ QDs are also very narrow, which is originated from the highly controllable and efficient synthesis by our technique. It is well-known that the FWHM could reflect the distribution condition of the PQDs in size and morphology. The narrower the FWHM, the more uniform the resulting PQDs. On the other hand, the FWHM is also a significant index to evaluate the monochromaticity of the materials. The narrower the FWHM, the better the monochromaticity (an important parameter estimated in LED lighting or display techniques) of the PQDs. As shown in Figures 2b and S2b, the emission spectrum peaks of the $CsPbX_3$ QDs can be tuned well from 408 to 694 nm by changing the ratio of halides effectively to realize entire visible spectra. After the calculation according to the previous method by comparing the samples with the standard fluorescent dyes (see the details in the Section 2),[28] the QY of the $CsPbX_3$ PQDs is in the range of 40−95% (see Figure S2c) and the highest QY is generated from the $CsPbBr_3$ QDs, which is the highest QY value ever reported for the $CsPbX_3$ PQDs in a colloidal solution sample. The narrow FWHM and high QY are mainly originated from the highly controllable synthesis, including the optimization of the synthesis condition, for example, reaction temperature, reaction time, ligand selection,

ligand ratio, and, mostly important, the hot injection technique, and the relative details will be discussed hereinafter.

3.2. Theoretical Band Structure of the Mixed-Halide Inorganic PQDs. In addition, we have calculated the band structures of the synthesized $CsPb(Br_xCl_{1-x})_3$ and $CsPb(I_xBr_{1-x})_3$, with $x = 0$, 1/3, 1/2, 2/3, and 1, PQDs based on the first-principle theory. Owing to the heavy lead element, the SOC and scalar relativistic terms are included in the density functional theory to accurately describe the band structures. Figure 3 shows the band structures of single- and mixed-halide semiconductors, SOC band gaps, the corrected band gaps, and the position of peak in PL spectra. It is found that the band gaps of mixed-halide all-inorganic PQDs are underestimated compared with the experimental emission peaks due to the nature of density functional theory. Therefore, to right characterize the changed trend of the band gaps, we use the alloy formula[17] to correct theoretically calculated results. As presented in Figure 3j, the band gaps of the generalized gradient approximation (GGA) with SOC corrected by the alloy formula are close to the experimental values, where the small differences between the simulation and experiment are mainly attributed to the changed size for different mixed-halide PQDs, as depicted in the XRD patterns and the small $1 \times 1 \times 2$ supercell models. Interestingly, the band structures of mixed-halide inorganic PQDs still own the direct transition character at the R point except the equal concentration, where the transition point is located at the M point. It is well-known that the direct band gap can improve the photoabsorption coefficient and accelerate the radiative recombination rate, which may explain the reason of high quantum yield in photoemission spectra for mixed-halide inorganic PQDs. Last but not the least, as shown in Figure 1, we stress that although the crystal structures are slightly distorted in contrast with the pure halide PQDs due to the halide ionic radius difference, making the bond length of $Pb^{2+}X^-$ change, the theoretical results and the good optical properties support that the synthesized $CsPbX_3$ PQDs with our improved hot injection technique possess relatively high sample quality.

3.3. Influences of the Synthesis Temperature and Time on the Optical Properties of the PQDs. In fact, the optical properties of the zero-dimension QDs could also be influenced by the surface groups. It is also well-accepted that the content percentage of the surface ligand adsorbed onto the QDs is thermodynamics process.[29] Here, we selected the optical property of the prepared $CsPbBr_3$ PQDs as a model to study the temperature-dependent surface influence. As shown in Figure S3, when the temperature was elevated from 140 to 180 °C, the PL intensity was increased gradually, which is because the emissive efficiency is directly in relation to the nonradiative decay, and, fortunately, the surface ligands could effectively passivate the surface defects. As discussed in the Section 1, the amount of surface ligands binding on the PQDs plays a very vital role in the optical property of the PQDs. The increased PL intensity with the reaction temperature increasing from 140 to 180 °C demonstrates that the amount of the ligands can be adjusted by the reaction temperature. However, when the temperature was elevated to higher than 180 °C (e.g., 200 °C), the PL intensity of the prepared PQDs was decreased. Furthermore, when the temperature was continued to be elevated to 220 °C, the fluorescence of the PQDs was absolutely quenched. Because the boiling point of oleic acid is ~195 °C, when the reaction temperature was elevated higher than this temperature, the effective concentration of oleic acid
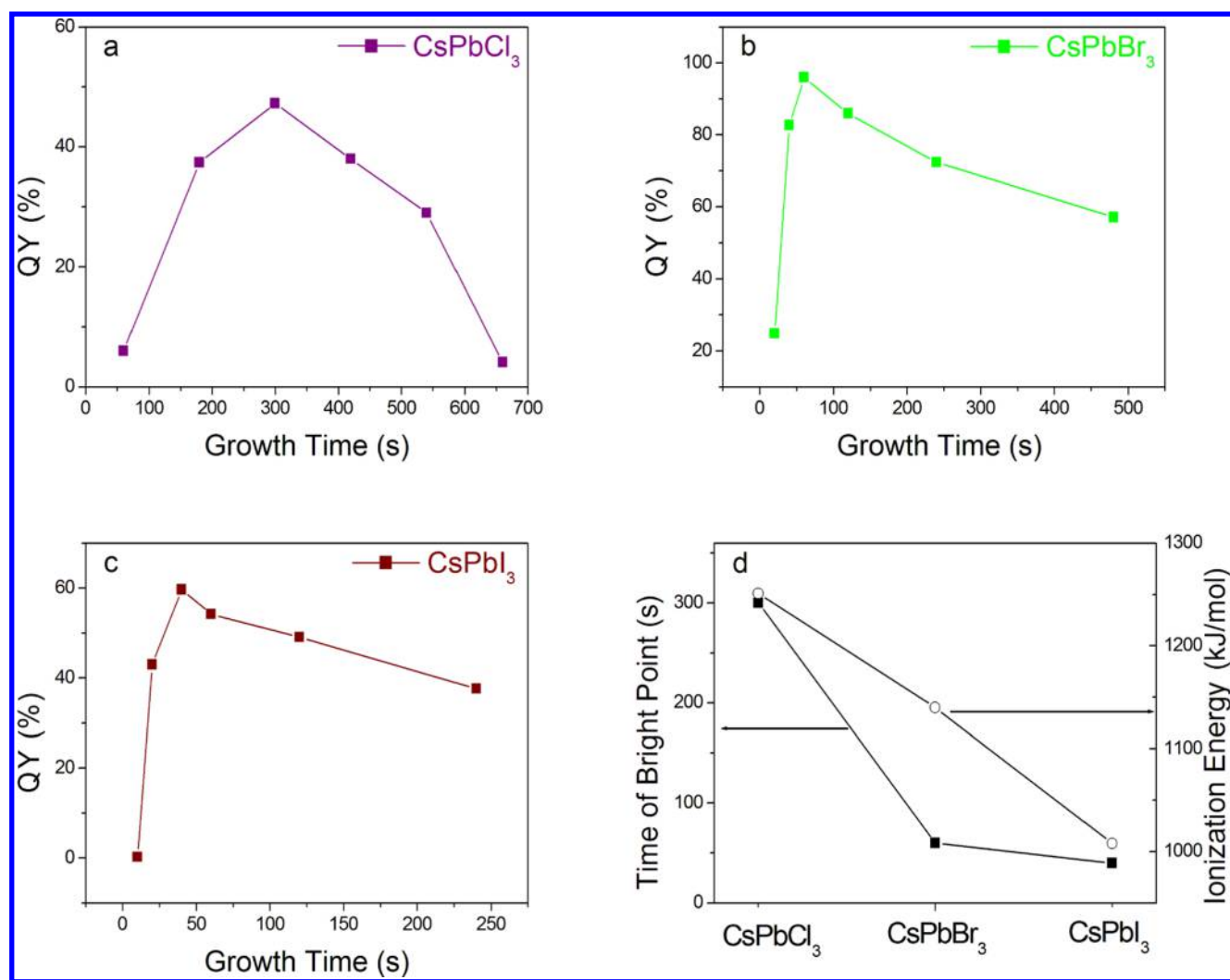
Figure 4. PL QY of $CsPbCl_3$ (a), $CsPbBr_3$ (b), and $CsPbI_3$ (c) PQDs vs PQDs' growth time. (d) Ionization energy and time of bright point vs the three PQDs.

would be greatly decreased and the reaction condition would be changed obviously. As a result, the optical property of the resulting $CsPbBr_3$ PQDs will be negatively influenced greatly, evidenced by the obvious decrease of the PL intensity. As shown in Figure S3, the shoulder peak in the PL spectra was obtained when the temperature was lower than 180 °C, for example, 140 or 160 °C, which is due to the appearance of the small-size PQDs once the temperature was decreased. The mixture of differently sized PQDs leads to non-Gaussian distribution PL spectra.

Apart from the reaction temperature, the reaction time is also an important issue to affect the optical property of the $CsPbX_3$ PQDs. In this work, we have systemically investigated the time-dependent PL spectra and QY of the $CsPbX_3$ (X = Cl, Br, and I) PQDs to optimize the reaction condition and reveal the importance of reaction time. Figure 4 shows that there is a turning bright point (the highest QY during the reaction time) of the three $CsPbX_3$ (X = Cl, Br, and I) PQDs when the reaction time was extended. Differently, from Cl to Br and to I, the turning bright point decreased from 300 to 60 s and to 30 s, which is because the ionization energy of the halogen ions is decreased from Cl^- (1251 kJ/mol) to Br^- (1140 kJ/mol) and to I^- (1008 kJ/mol) successively (shown in Figure 4d). Therefore, the reaction time was shortened successively from

$CsPbCl_3$ to $CsPbBr_3$ and to $CsPbI_3$ PQDs. Anyway, there is an optimal reaction time for each $CsPbX_3$ (X = Cl, Br, and I) PQD, respectively, rather than a uniform reaction time as introduced previously for all $CsPbX_3$ (X = Cl, Br, and I) PQDs.[15]

3.4. Comparison of the Photostability of the $CsPbX_3$ PQDs Synthesized by Our Method versus the Method via Anion Exchange. Compared with the traditional mixed-halide $CsPbX_3$ PQDs prepared by the anion-exchange process at 40 °C, the mixed-halide $CsPbX_3$ PQDs prepared via our method present a higher photostability, which is very important in the applications of photoelectric devices.[5−8] As shown in Figure 5, the $CsPbX_3$ PQDs synthesized by our method show improved stability with the ultraviolet lamp exposure. In contrast, the $CsPbX_3$ PQDs prepared via anion exchange by the previous method[15] show a weak photostability because the phase separation (including the distortion of the cubic phase and expansion or shrinkage of the lattice constant) would lead to the change of the optical property, especially leading to poor stability.[16] Therefore, it can be seen from Figure 5a,b that as the irradiation time was extended, both the absorption and PL spectra dropped rapidly. However, the $CsPbX_3$ PQDs synthesized by our method show strong photostability. With the passage of time, both the absorption and PL spectra kept
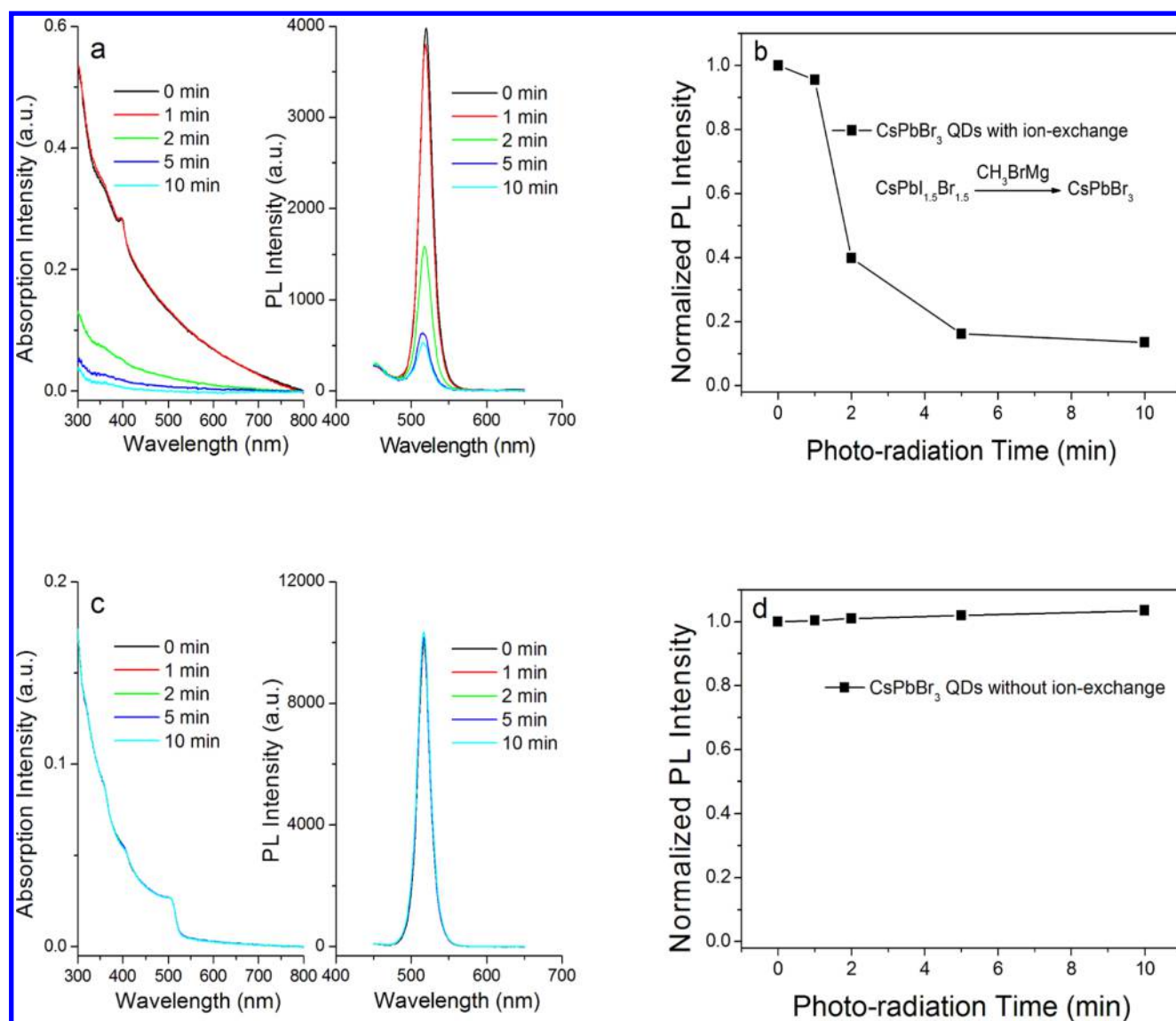
Figure 5. Absorption and PL spectra of $CsPbX_3$ PQDs obtained via anion exchange (a) or without anion exchange (c) under 365 nm ultraviolet lamp photoradiation at different times. (b, d) Normalized PL intensity of the relative PL spectra vs the photoradiation time. The $CsPbX_3$ PQDs obtained via anion exchange were obtained by reacting $CsPbI_{1.5}Br_{1.5}$ PQDs with methylmagnesium bromide. The $CsPbX_3$ PQDs without anion exchange are the $CsPbBr_3$ PQDs prepared by our method.

almost constant (see Figure 5c,d). These results prove sufficiently that the photostability of the PQDs prepared by our method is superior to that of the PQDs obtained by the anion-exchange technique, which further demonstrates that the surface of our PQDs is rather stable due to the highly efficient surface ligand coordination process.

4. CONCLUSIONS

In summary, the single- and mixed-halide $CsPbX_3$ PQDs were synthesized via the hot injection technique. The surface ligands were strongly coordinated onto the surface of the PQDs, hence optimizing the optical properties and improving the stability of the resulting $CsPbX_3$ PQDs. The friendly double ligands OA/OAm were used instead of the traditional OA/OAm/TOP mixture to synthesize the PQDs. As compared with the previous strict synthesis processes that needed vacuumization or/and glovebox equipment, our method is rather simple to prepare high-quality PQDs through accurately controlling the ratio of different halide atoms and the hot injection technique.

The resulting PQDs have high QY (40−95%), narrow FWHM (the narrowest FWHM <10 nm), tunable band gap (408−694 nm) in the entire-visible-light window, and most importantly strong photostability, which will bring wide applications for PQDs in photoelectric devices, such as LEDs and solar cells. Furthermore, first-principle theory calculations support our experimental results that the high QY of PQDs may be due to the direct band gaps for mixed-halide PQDs and show that the theoretical band gaps corrected by the alloy formula are in good agreement with the emission peaks in PL spectra. Hence, these PQDs show great potential as good candidates for the photoelectric devices in the future.

■ ASSOCIATED CONTENT

⑤ Supporting Information

The Supporting Information is available free of charge on the ACS Publications website at DOI: 10.1021/acsami.7b10612.

Schematic presentation of the synthesis of CsPbX$_3$ PQDs (Figure S1), the FWHM, PL peak position, and QY of the CsPbCl$_3$, CsPbBrCl$_2$, CsPbBr$_{1.5}$Cl$_{1.5}$, CsPbBr$_2$Cl, CsPbBr$_3$, CsPbIBr$_2$, CsPbI$_{1.5}$Br$_{1.5}$, CsPbI$_2$Br, and CsPbI$_3$ PQDs shown in Figure 2 (Figure S2), absorption and emission spectra of CsPbBr$_3$ PQDs prepared at different temperatures (Figure S3), and elemental composition of Cs, Pb, Cl, Br, and I atoms of the relative samples calculated by the EDS results from Figure 1c (Table S1) (PDF)

■ AUTHOR INFORMATION

Corresponding Author

*E-mail: qhzeng@ciomp.ac.cn.

ORCID ⊙

Wenyu Ji: 0000-0003-2932-5119

Qinghui Zeng: 0000-0002-1211-3980

Author Contributions

§Y.S. and X.C. contributed equally to this work.

Notes

The authors declare no competing financial interest.

■ REFERENCES

(1) Gao, X. H.; Cui, Y. Y.; Levenson, R. M.; Chung, L. W. K.; Nie, S. M. In Vivo Cancer Targeting and Imaging with Semiconductor Quantum Dots. *Nat. Biotechnol.* **2004**, *22*, 969−976.

(2) Dai, X.; Zhang, Z. X.; Jin, Y. Z.; Niu, Y.; Cao, H. J.; Liang, X. Y.; Chen, L. W.; Wang, J. P.; Peng, X. G. Solution-Processed, High-Performance Light-Emitting Diodes based on Quantum Dots. *Nature* **2014**, *515*, 96−99.

(3) Shen, H. B.; Bai, X. W.; Wang, A.; Wang, H. Z.; Qian, L.; Yang, Y. X.; Titov, A.; Hyvonen, J.; Zheng, Y.; Li, L. S. High-Efficient Deep-Blue Light-Emitting Diodes by Using High Quality Zn$_x$Cd$_{1-x}$S/ZnS Core/Shell Quantum Dots. *Adv. Funct. Mater.* **2014**, *24*, 2367−2373.

(4) Shen, H.; Cao, W. R.; Shewmon, N. T.; Yang, C. C.; Li, L. S.; Xue, J. G. High-Efficiency, Low Turn-on Voltage Blue-Violet Quantum-Dot-Based Light-Emitting Diodes. *Nano Lett.* **2015**, *15*, 1211−1216.

(5) Song, J.; Li, J. H.; Li, X. M.; Xu, L. M.; Dong, Y. H.; Zeng, H. B. Quantum Dot Light-Emitting Diodes Based on Inorganic Perovskite Cesium Lead Halides (CsPbX$_3$). *Adv. Mater.* **2015**, *27*, 7162−7167.

(6) Zhang, F.; Zhong, H. Z.; Chen, C.; Wu, X. G.; Hu, X. M.; Huang, H. L.; Han, J. B.; Zou, B. S.; Dong, Y. P. Brightly Luminescent and Color-Tunable Colloidal CH$_3$NH$_3$PbX$_3$ (X = Br, I, Cl) Quantum Dots: Potential Alternatives for Display Technology. *ACS Nano* **2015**, *9*, 4533−4542.

(7) Wang, Y.; Li, X. M.; Nalla, V.; Zeng, H. B.; Sun, H. D. Solution-Processed Low Threshold Vertical Cavity Surface Emitting Lasers from All-Inorganic Perovskite Nanocrystals. *Adv. Funct. Mater.* **2017**, *27*, No. 1605088.

(8) Swarnkar, A.; Marshall, A. R.; Sanehira, E. M.; Chernomordik, B. D.; Moore, D. T.; Christians, J. A.; Chakrabarti, T.; Luther, J. M. Quantum Dot-Induced Phase Stabilization of Alpha-CsPbI$_3$ Perovskite for High-Efficiency Photovoltaics. *Science* **2016**, *354*, 92−95.

(9) Wuister, S. F.; Donega, C. D. M.; Meijerink, A. Luminescence Temperature Antiquenching of Water-Soluble CdTe Quantum Dots: Role of the solvent. *J. Am. Chem. Soc.* **2004**, *126*, 10397−10402.

(10) Zeng, Q.; Zhang, Y.; Xue, B.; Liu, K.; An, L.; Tu, L.; Liu, X.; Kong, X. Controlling the Fluorescent Properties of Aqueous CdTe Nanocrystals by Modulating the Growth Rate. *J. Nanosci. Nanotechnol.* **2013**, *13*, 858−863.

(11) Majetich, S. A.; Carter, A. C. Surface Effects on the Optical-Properties of Cadmium Selenide Quantum Dots. *J. Phys. Chem.* **1993**, *97*, 8727−8731.

(12) Talapin, D. V.; Haubold, S.; Rogach, A. L.; Kornowski, A.; Weller, H. A Novel Organometallic Synthesis of Highly Luminescent CdTe Nanocrystals. *J. Phys. Chem. B* **2001**, *105*, 2260−2263.

(13) Talapin, D. V.; Rogach, A. L.; Kornowski, A.; Haase, M.; Weller, H. Highly Luminescent Monodisperse CdSe and CdSe/ZnS Nanocrystals Synthesized in a Hexadecylamine-Trioctylphosphine Oxide-Trioctylphospine Mixture. *Nano Lett.* **2001**, *1*, 207−211.

(14) Pradhan, N.; Reifsnyder, D.; Xie, R. G.; Aldana, J.; Peng, X. G. Surface Ligand Dynamics in Growth of Nanocrystals. *J. Am. Chem. Soc.* **2007**, *129*, 9500−9509.

(15) Nedelcu, G.; Protesescu, L.; Yakunin, S.; Bodnarchuk, M. I.; Grotevent, M. J.; Kovalenko, M. V. Fast Anion-Exchange in Highly Luminescent Nanocrystals of Nesium Lead Halide Perovskites (CsPbX$_3$, X = Cl, Br, I). *Nano Lett.* **2015**, *15*, 5635−5640.

(16) Protesescu, L.; Yakunin, S.; Bodnarchuk, M. I.; Bertolotti, F.; Masciocchi, N.; Guagliardi, A.; Kovalenko, M. V. Monodisperse Formamidinium Lead Bromide Nanocrystals with Bright and Stable Green Photoluminescence. *J. Am. Chem. Soc.* **2016**, *138*, 14202−14205.

(17) Yin, W. J.; Yan, Y.; Wei, S. H. Anomalous Alloy Properties in Mixed Halide Perovskites. *J. Phys. Chem. Lett.* **2014**, *5*, 3625−3631.

(18) Brivio, F.; Caetano, C.; Walsh, A. Thermodynamic Origin of Photoinstability in the CH$_3$NH$_3$Pb(I$_{1-x}$Br$_x$)(3) Hybrid Halide Perovskite Alloy. *J. Phys. Chem. Lett.* **2016**, *7*, 1083−1087.

(19) Jong, U. G.; Yu, C. J.; Ri, J. S.; Kim, N. H.; Ri, G. C. Influence of Halide Composition on the Structural, Electronic, and Optical Properties of Mixed CH$_3$NH$_3$Pb(I$_{1-x}$Br$_x$)(3) Perovskites Calculated Using the Virtual Crystal Approximation Method. *Phys. Rev. B* **2016**, *94*, No. 125139.

(20) Kresse, G.; Furthmuller, J. Efficiency of Ab-Initio Total Energy Calculations for Metals and Semiconductors Using A Plane-Wave Basis Set. *Comput. Mater. Sci.* **1996**, *6*, 15−50.

(21) Kresse, G.; Furthmuller, J. Efficient Iterative Schemes for Ab Initio Total-Energy Calculations Using A Plane-Wave Basis Set. *Phys. Rev. B* **1996**, *54*, 11169−11186.

(22) Perdew, J. P.; Burke, K.; Ernzerhof, M. Generalized Gradient Approximation Made Simple. *Phys. Rev. Lett.* **1996**, *77*, 3865−3868.

(23) Blochl, P. E. Projector Augmented-Wave Method. *Phys. Rev. B* **1994**, *50*, 17953−17979.

(24) Kresse, G.; Joubert, D. From Ultrasoft Pseudopotentials to the Projector Augmented-Wave Method. *Phys. Rev. B* **1999**, *59*, 1758−1775.

(25) Protesescu, L.; Yakunin, S.; Bodnarchuk, M. I.; Krieg, F.; Caputo, R.; Hendon, C. H.; Yang, R. X.; Walsh, A.; Kovalenko, M. V. Nanocrystals of Cesium Lead Halide Perovskites (CsPbX$_3$, X = Cl, Br, and I): Novel Optoelectronic Materials Showing Bright Emission with Wide Color Gamut. *Nano Lett.* **2015**, *15*, 3692−3696.

(26) Akkerman, Q. A.; Motti, S. G.; Kandada, A. R. S.; Mosconi, E.; D'lnnocenzo, V.; Bertoni, G.; Marras, S.; Kamino, B. A.; Miranda, L.; De Angelis, F.; Petrozza, A.; Prato, M.; Manna, L. Solution Synthesis Approach to Colloidal Cesium Lead Halide Perovskite Nanoplatelets with Monolayer-Level Thickness Control. *J. Am. Chem. Soc.* **2016**, *138*, 1010−1016.

(27) Swarnkar, A.; Marshall, A. R.; Sanehira, E. M.; Chernomordik, B. D.; Moore, D. T.; Christians, J. A.; Chakrabarti, T.; Luther, J. M. Quantum Dot-Induced Phase Stabilization of A-CsPbI$_3$ Perovskite for High-Efficiency Photovoltaics. *Science* **2016**, *354*, 92−95.

(28) Grabolle, M.; Spieles, M.; Lesnyak, V.; Gaponik, N.; Eychmuller, A.; Resch-Genger, U. Determination of the Fluorescence Quantum

Yield of Quantum Dots: Suitable Procedures and Achievable Uncertainties. *Anal. Chem.* **2009**, *81*, 6285−6294.

(29) Zeng, Q. H.; Xue, B.; Zhang, Y. L.; Wang, D.; Liu, X. M.; Tu, L. P.; Zhao, H. F.; Kong, X. G.; Zhang, H. Facile Synthesis of NaYF$_4$:Yb, Ln/NaYF$_4$:Yb Core/Shell Upconversion Nanoparticles Via Successive Ion Layer Adsorption and One-Pot Reaction Technique. *CrystEngComm* **2013**, *15*, 4765−4772.